Master's Thesis

Antireflection Patterning of Si for InAsSb Nanowire Infrared Photodetectors

By

Muhammad Rizwan Khalid

Supervisor

Johannes Svensson

Department of Physics
Lund University
Sweden

Abstract

The pattering of an optical surface with physical features like with very low reflectivity and high transmission of IR or visible light can be used e.g. for antireflective windows for solar cells and photodetectors. Here we present results on antireflective patterning of Si for back side illuminated InAsSb nanowire long wavelength IR (8-15 μm) photodetectors. Photolithography and dry etching techniques are used to pattern Si into uniform pillars and by using a Fourier transform infrared spectrometer we measure the transmittance. We use numerical simulations to aid the design of the dimensions of Si pillars. Results from transmittance measurements exhibit diameter dependent peaks that are in good agreement with the numerical simulations. The numerical results reveal that the transmission peaks are due to resonant wave guiding modes that enhance the coupling of light into the Si pillars. We have found that with the proper selection of pillar diameter a resonance enhanced transmission peak at specific wavelength can be achieved. We have found that the transmission of IR through bared Si is 53% which is independent of wavelength. Arrays of Si pillars with mean diameter 1.33 μm ± 36 nm show transmission peak at wavelength of 6.2 μm and array of Si pillars having mean diameter 1.42 μm ± 35 nm shifts the transmission peak at wavelength of 7.5 μm. Doughnut shaped Si hollow pillars are also observed as a result of photolithography. The transmission spectrum of Si hollow pillar arrays is also analyzed.

ACKNOWLEDGEMENTS

The whole praise to Allah, the Sovereign power, who made me the super creature, blessed me with knowledge, and enabled me to accomplish this task. I offer my humblest and sincerest words of thanks to his Holy Prophet Muhammad (PBUH) who is forever a source of guidance for humanity.

There are numerous people who helped me in carrying out the project and it would have been very difficult to finish it without their kind support and guidance. The work presented in this thesis has been done under the supervision of Mr. Johannes Svensson ‘‘Nano Electronics group, Electrical and Information Technology, Lund University’’ (johannes@eit.lth.se). He was a great source of inspiration and guidance to me. He supported me throughout the thesis duration with his knowledge and guidance to keep me on the right track and always managed time for me despite of his busy schedule. He is not only a remarkable scientist but a very nice person also.
His valuable suggestion will always serve as beacon of light throughout the course of my study.

I am highly indebted to Professor Mr. Lars-Erik Wernersson ‘‘Head Nano-electronics group, EIT, Lund University,’’ who gave me the chance to work on this project and be part of a prestigious research group.

I wish to express my deepest obligation to my Parents. I am hard pressed for words to extend my gratitude for their care and support. They helped and guided me through all the difficult phases of life and nurtured me to become a better person. I am grateful to my brothers and sisters for their prayers and encouragement to carry out my studies with devotion.

A word of special gratitude to my friends for their help through various stages of my thesis.

I pay invaluable gratitude to Mr. Tomas Brage ‘‘Director of studies, Physics Department, Lund University,’’ for his help and guidance at different stages during my MSc Physics at Lund University.

List of Figures

Table of Contents

Page

1. INTRODUCTION

1.1 Introduction

The interaction of light with matter is one of the most significant physical processes that has very strong applications and implications in our daily life. For example photosynthesis, photovoltaic effect, photoconductor and electroluminescent process all involve the light matter interaction. In photosynthesis plants convert sun light into chemical energy. The photovoltaic effect is used to convert sun light directly into electrical energy; this effect is the basis of solar cells. In photoconductive effect the resistance of a sample is reduced by the absorption of incident light; this effect is used in photo detectors. The reciprocal of photovoltaic effect is electroluminescence in which electric energy is directly transferred to the emitted photons; this effect is used in light emitting diodes.

Different surface antireflection techniques are used to improve the performance of optical and optoelectronic devices such as photo-detectors, solar cells and many other sensing devices [2]. Usually thin films have been used to minimize the reflection of electromagnetic radiation from optical surfaces, but lately the use of antireflection structured surfaces has been introduced [3]. By using the deep surface texturing of several micrometers with a sub-wavelength periodic pattern on an optical surface e.g. silicon one can minimize the surface reflection over a broad spectral range [2].Surface patterning is a more precise and effective solution for reducing light reflection losses as compared with antireflection coating. For surface patterning reactive ion etching (RIE) can be effectively used [1].

Periodic structure on an optical surface can control the light diffraction properties and also behavior of photon due to its photonic band gap, so these properties of periodic structures can enhance absorption of light. By shaping these structures in the form of nano-pillars or pyramids one can also achieve the resonance enhanced optical absorption [4].

The purpose of this work is to study the resonance enhanced transmission of long wavelength infra-red (LWIR) through silicon (Si) antireflective structures.

1.2 Background

1.2.1 Antireflective patterning of silicon surface

The first anti-reflective coating was discovered more than 70 years ago by a Ukrainian Scientist working for Zeiss in Germany [5]. In our work the targeted material is silicon; with this in mind we mainly focus on the work that has been done on its surface in this field. Silicon is the most lavish material on the earth crust after oxygen and the most widely available semiconductor material. It is relatively cheap and also a well understood material for producing microelectronics devices. Si photonics is not completely developed as compared to the direct band gap III-V semiconductor

photonics [6]. However, in recent years serious research progress has been made in silicon photonics and antireflective gratings have been widely investigated with the emergence of photovoltaic and photo sensing. Different kinds of antireflective coatings can be used. First optical thin films are widely used to achieve low reflectivity over a large and tunable band of wavelength.

Secondly arrays of microstructures are used to reduce reflection of the surface which is inspired by the antireflective properties on the surface of the eye of a moth [7]. In 1973, P. H. Clapham et al. observed that some insects have micro-structures on the surface of their eyes which act as an antireflective surface. With the help of these patterned antireflective structures they have achieved enhanced night vision abilities [8]. There are many fundamental parameters of these structures which can influence the optical response e.g. size, shape and arrangements. Variations in these parameters offer a large tunable antireflective band. Random structures on silicon surface, usually known as black silicon, also give a broad range of antireflective band; to predict its optical properties is a big computational task [7]. Black silicon was discovered in the 1980s as an unwanted secondary effect of reactive ion etching. It has very low reflectivity and correspondingly high absorption of visible and infrared light.

1.2.2 Infra-red radiation

Fredrick William Hershel (1738-1822) did experiments with a thermometer and a prism about 213 years ago and for the first time infrared radiation was reported [21]. He found that this radiation was reflected, refracted, absorbed and transmitted just like visible light [22]. The electromagnetic spectrum covers a wide range of wavelengths. The wavelength band of infrared radiation is located between visible light and microwaves at approximately 780nm to 1mm as can be seen in fig.1.1.

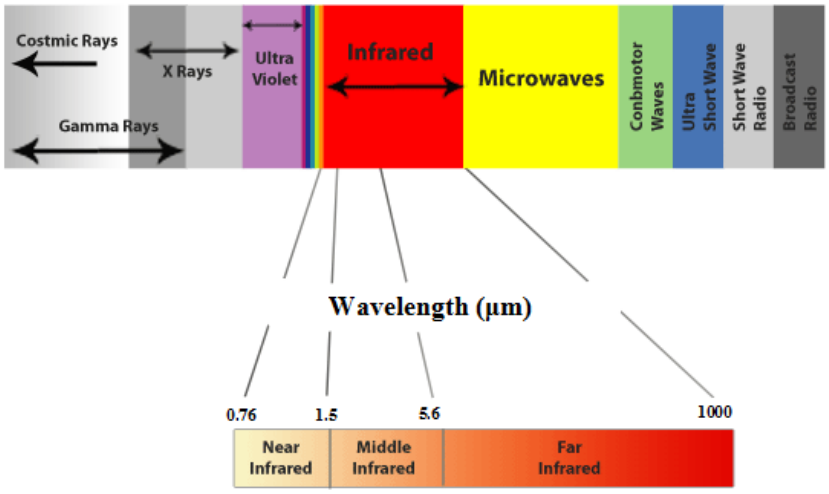

Figure 1.1 *Electromagnetic spectrum showing broad band infrared radiation regimes [39].*

The infra-red spectrum can be classified in different regions as in table 1;

Table 1.1. Classification of infra-red spectrum

No	Division Name	Wavelength (µm)
1	Near Infra-red (NIR)	0.78-1.4
2	Mid wavelength Infra-red (MIR)	2 -7
3	Long wavelength infrared (LWIR)	8 -15
4	Far infra-red (FIR)	15 -1000

1.3 Applications

Unusual broad band antireflection properties of a material textured surface, combined with the semiconductor properties of Si makes this material interesting for a wide variety of applications; these surfaces are used to improve the sensitivity of photo detectors, to increase the performance of light emitting diodes and also to enhance the efficiency of photovoltaic cells etc. [9].

1.3.1 Photo-detectors

To detect photons many different semiconductor devices can be used, known as photo detectors. In 1971, the first infrared photoconductor was developed by Case [23]. The development of modern IR detector technology started during the years of World War II. The wavelength of two atmospheric windows 3-5 and 8-14µm with low absorption was the main interest; important developments have been done in that area. In recent years more interest has been focused on long wavelength infrared detectors motivated by space applications [24].

The basic principle of photo detectors is very simple; they convert optical signals into electrical signals. The conductivity of the material is increased when large number of electrons and holes are generated in a semiconductor. The change of conductivity in a semiconductor is the basis of the simplest type of photo detector. When electrons and holes are generated within the space charge region of a pn-junction they are separated by the electric field and a current is produced. This signal gives the information about the incident photon. Most of the photodetectors including photodiodes and phototransistors basically consist of a pn-junction [25].

IR-detectors are usually classified in different groups depending upon their materials and efficiency [26].

Infrared detectors are used as optical power meters, radiation thermometers, flame monitors, moisture analyzers, gas analyzers, infrared imaging devices, remote sensing, human body detection etc.

1.3.2 Solar cells

Chapin et al. at Bell labs in 1954 had invented, discovered and demonstrated the first Si single crystal solar cell with the efficiency of 6%. After that developments have been made by researchers and brought the efficiency up to 15% [27].

A solar cell basically consists of a pn-junction at which no direct voltage is applied across the junction. It converts solar power into electrical power. There are different types of solar cells like pn-junction, heterojunction and amorphous silicon cells.

In a simple pn-junction solar cell photon illumination creates electron hole pairs in the space charge region. These will be swept out and produce a photocurrent in the junction reverse biased direction [25].

1.4 Goal

The final objective of this project is to find the resonance enhanced wavelength specific transmission of long wavelength infrared light by patterning a silicon surface. These patterns will be used in back side illuminated InAsSb nanowire infrared photodetectors.

2. THEORY

2.1 Electromagnetic wave propagation in linear media

The behavior of electromagnetic waves is usually described by Maxwell's equations. For a linear and homogeneous medium with

$$D = \boldsymbol{\varepsilon E} \qquad (2.1)$$

$$B = \mu H \qquad (2.2)$$

where, E represents electric field, B Magnetic field, $\boldsymbol{\varepsilon}_{(0)}$ permittivity of (free) space (dielectric tensor), $\mu_{(0)}$ permeability of (free) space (magnetic tensor), and D electric displacement,

The reduced form of Maxwell's equations are;

(i) $\nabla \bullet D = \rho$ (2.3)

(ii) $\nabla \bullet B = 0$ (2.4)

(iii) $\nabla \times E = -\frac{\partial B}{\partial T}$ (2.5)

(iv) $\nabla \times H = J + \frac{\partial D}{\partial t}$ (2.6)

Here, $\nabla \bullet$ is the divergence operator, $\boldsymbol{\nabla}\times$ the curl operator field, J free current density and ρ free charge density.

The speed of electromagnetic waves through a linear and homogeneous medium;

$$v = \frac{1}{\sqrt{\varepsilon\mu}} = \frac{c}{n} \qquad (2.7)$$

n is refractive index of material;

$$n = \sqrt{\frac{\varepsilon\mu}{\varepsilon_o \mu_o}} \qquad (2.8)$$

If permeability of free space is mostly equal to the permeability of material, so equation (2.8) would become;

$$n = \sqrt{\varepsilon_r} \qquad (2.9)$$

ε_r is the relative permittivity or dielectric constant of the material. It is a well-known fact of optics that light passes at lower speed through matter as compared with free space; as a result ε_r is always greater than 1 [11].

2.2 Light matter interaction

We need to know how enhance transmission and tune the way light interacts with the sample. The simplest way of light propagation in a macroscopic bulk sample is in the

form of plane wave. Such a kind of light wave propagation in optics simplifies the analysis of the optical response. But in other cases when an optical surface is textured with geometrical features at a length scale similar to the wavelength of incident light, a tunable light propagation could be achieved.

Thus in a Si pillar array of diameter *D* with pitch *P* and length *L* (Fig. 2.1), a more complicated type of light propagation could be expected. By varying these three parameters one can get different optical response of the pillars [10]. The pitch *P* is the distance between the centers of two consecutive pillars.

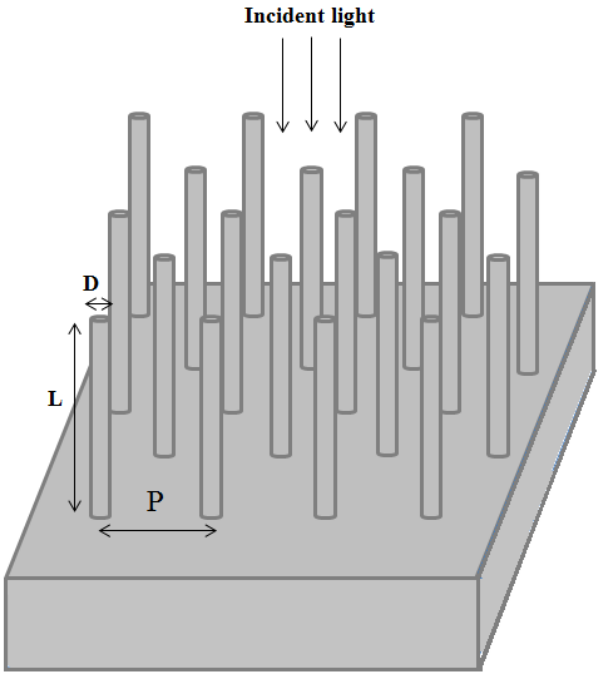

Figure 2.1 *A schematic of vertical Si-pillars of pitch P, diameter D and length L. The light is incident at normal angle to the array propagating parallel to the axis of Si-pillars.*

A full electrodynamic description is needed to understand the interaction of incident light with array of pillars; however simple effective medium theories cannot describe it properly. Consider that the light is incident at normal angle to the pillar array i.e. the light propagates parallel to the pillar axis. Its electric field is perpendicular to the pillar axis. In the case when we are dealing with long wavelength limit, ($D, P << \lambda$), a new expression for the effective dielectric constant ε_{eff} can be found [34]

$$\varepsilon_{eff} = [\varepsilon_P + 1 + f(\varepsilon_P - 1)]/[\varepsilon_P + 1 - f(\varepsilon_P - 1)] \qquad (2.10)$$

where ε_P is the dielectric constant of the Si pillar, f is the volume fraction occupied by the pillars [35]

$$f = \pi\left[\left({}^{D}/_{2}\right)/P\right]^2 \qquad (2.11)$$

optical response of pillars depends on the filling factor *f* and also on the *D*, *P*.

2.3 Reflectance and transmittance at normal incidence

When light is incident on an interface between two non-absorbing materials, some part of that light is reflected and some part is transmitted. The reflected light is denoted by I_R, the transmitted part of light I_T and the intensity of incident light I_I.

The reflection coefficient R and transmission coefficient T are defined by the following ratios

$$R = \frac{I_R}{I_I} = \left(\frac{E_{OR}}{E_{OI}}\right)^2 = \left(\frac{n_1 - n_2}{n_1 + n_2}\right)^2 \qquad (2.12)$$

(2.12) is the well-known Fresnel relation for the fraction R of light intensity reflected at normal incidence. E_{OI}, E_{OR} and E_{OT} represent the complex amplitude of E for incident, reflected and transmitted electromagnetic plane wave respectively.

The ratio of transmitted intensity to the incident intensity is

$$T = \frac{I_T}{I_I} = \frac{\varepsilon_2 v_2}{\varepsilon_1 v_1}\left(\frac{E_{OT}}{E_{OI}}\right)^2 = \frac{4n_1 n_2}{(n_1 + n_2)^2} \qquad (2.13)$$

n_1 and n_2 are the index of refraction whereas ε_1 or ε_2 is called the relative permittivity or the dielectric constant of the material respectively. Reflectance R and transmittance T depend on angle of incidence, interference effects as well as the refractive indices of both materials [11].

It is not easy to calculate the reflectance and transmittance when more than one interface is involved. Because the measurements of reflectance and transmittance are obtained from the whole device not from a single interface, each interface contributes to the measurement. This makes the characterization of the device very complicated. Reflectance R and transmittance T are normally given in percentage. In case of more than one interface the following relation holds only when the absorption coefficient $\alpha=0$.

$$T + R = 1 \qquad (2.14)$$

For all interfaces the sum of reflectance R and transmittance T should be equal to unity as of course conservation of energy requires.

2.4 Optical properties of Si pillars

The abundance of silicon on earth increases its importance as an economic semiconductor for optoelectronics applications. The optical properties of the Si microstructures are particularly sensitive to their physical dimensions.

The optical properties of Si strongly depend on whether the Si pillars absorb or transmit the light. Si has an indirect band gap of 1.1 eV at 300 K [28], and absorbs only wavelengths with higher photon energy than the Si band gap. If the photon energy is smaller than the band gap of Si then it will be transmitted through the sample.

The relationship between the energy E of photon and the wavelength λ of light is given by

$$E = \frac{hc}{\lambda} \tag{2.15}$$

Where h is Planck's constant and c is the speed of light.

The transmission properties of Si make it suitable for the infrared region. It was discovered that the periodic structure of nanowire array as compared with planes can exhibit outstanding antireflection properties because these periodic structures reflect a very small amount of light [10].

2.5 Diameter dependent structures

The optical properties of microstructures are particularly dependent on their physical dimensions [30]. The optical response of transmitting silicon pillars is determined to a large extent by the relation between the pillar diameter D and the wavelength λ of the incident light. The response can be divided into three different regimes, (i) $\lambda << D$, (ii) $D << \lambda$ and (iii) $D \approx \lambda$.

In the first case the interaction of light with Si pillars can be explained by geometrical optics and in second case the interaction can be described by electrostatics. In the electrostatic limit, due to the large contrast in the refractive index of air and pillar, the incident light is screened from the interior of the pillar. The third case is more important and interesting in our case; when $D \approx \lambda$, optical resonances can be observed [29]. These resonances can be used for tuning resonance enhanced transmission of infrared light through Si pillars.

2.6 Resonant enhanced transmission of infra-red

The wavelength specific absorption, reflection and transmission of vertical silicon microstructure arrays originate from the field distribution of fundamental HE_{11} wave guided mode which is highly wavelength dependent. The HE_{11} wave guided mode is supported by each silicon pillar.

Fig. 2.2 shows the possible interactions of light at normal incident with a silicon pillar. However, as discussed above, Si does not absorb long wavelength infrared (LWIR). Infrared radiation with specific wavelength interacts with pillars at the top air/pillar interface and is reflected or transmitted at the bottom silicon/pillar interface [30].

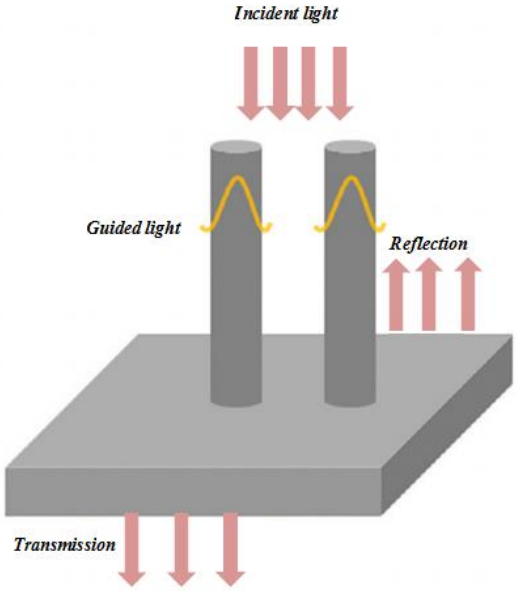

Figure 2.2 *A schematic of vertical silicon pillars of pitch P, diameter D and length L. The light is incident at normal angle to the array and propagates parallel to the axis of silicon pillars; an illustration of wavelength selective wave-guiding system [30].*

Since we are using a homogeneous medium for pillar and substrate, it was predicted that the reflectance of a plane wave decreases and transmittance increases with decreasing differences of refractive index between the media. If the difference of index between pillar and substrate is very low, then it is expected that the coupling between the pillar mode and substrate should increase which results in the higher rate of transmission and lower rate of reflectance [30]

3. FABRICATION

3 Fabrication

Photolithography is used to define the anti-reflective (AR) patterns and reactive ion etching (RIE) for etching the Si surface. This fabrication needs several critical manufacturing steps that are (a) Adhesion Promotion, (b) Resist coat, (C) Soft bake, (d) Alignment, (e) Exposure, (f) Development, (g) Inspection and Measurements, (h) Hard Bake, (i) Etching. Some important steps are discussed in the next sections.

3.1 Resist coat

The Si surface is first coated with a photoresist which is a light sensitive material. A photoresist typically consists of organic polymers applied from a solution. First a volume of liquid resist is distributed onto the sample's surface. Then the sample is spun by a high speed spinner. Excess resist is flying off leaving behind a thin film of resist, as schematics show in figure 3.1 (b). Afterwards, to improve the adhesion of resist and to make its density sufficient to support the later process, the sample is baked at about $115^{o}C$ to drive out the solvents from the thin film [12].

Different concentrations of resists are used to coat the surface having different thicknesses with respect to the spin speed; for example photo resist S1813 spun at 4000 rounds per minute (rpm) gives photoresist thickness 1.3 μm. Similarly S1811 and S1805 give photoresist thickness of 1.1 μm and 0.5 μm respectively at spin speed 4000 rpm [13].

Photoresists can be broadly classified in two different groups as positive or negative, depending on how it responds to radiation.

3.1.1 Positive resist

The exposed regions become more soluble and unexposed positive resists normally have very low solubility in the developer. The patterns made in positive resist after development are the same as those that are metal coated on the mask. There are three components of positive photoresist, "photosensitive compound, an organic solvent and a base resin". The photosensitive compound is sensitive to radiation and absorbs radiation in exposed areas. Radiation exposure changes its chemical structure to break its long polymer chains into parts that become soluble in a developer.

3.1.2 Negative resist

Negative resist behaves oppositely to the positive resist. Photosensitive compounds absorb radiation and after chemical reaction the polymers cross link with each other, resulting in a higher molecular weight to become insoluble in developer solution [14].

3.1.3 Limitations and disadvantages in resist coat

Mostly in coating thick resist films a so called edge bead forms which causes unwanted proximity-gap between mask and flat surface of the resist film during exposure. It forms due to the surface tension near the substrate edge. This effect may reduce the resolution of the exposure.

One more common effect can be seen in film deposition which is an uneven thickness of resist, typically comet-shaped. This effect is due to insufficient substrate cleaning or due to dust particles in the resist, air or N_2 bubbles beneath the resist film [15].

3.2 Photolithography

Photo lithography is the process of transferring patterns of geometrical shapes of a mask on a semiconductor surface covered with a photoresist. The mask aligner MJB4 (soft UV) "Suss Micro Tech.'' is used as a UV lithography system.

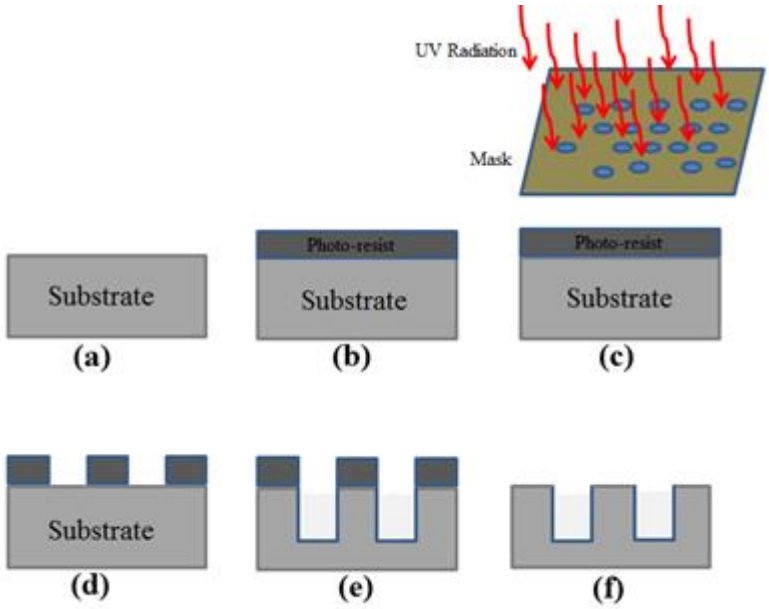

Figure 3.1 *Schematics showing the main steps in photolithography and etching process, (a) A clean Si Substrate, (b) photoresist application, (c) alignment and exposure, (d) exposed regions are developed by using MF319 solution, (e) Dry etching by using RIE (reactive ion etching), (f) Mask (resist) removal by using Acetone and Isopropanol.*

3.2.1 Alignment, exposure and development

Photolithography is followed by an etching process. The sample is aligned with respect to the mask as shown in fig. 3.1 (c). MJB4 can handle alignment accuracy around 1 µm or less and can reproduce features in the micrometer range. There are several different printing modes available on MJB4 and we have used a vacuum contact mode which gives the best resolution. In this mode of operation the gap between mask and substrate is evacuated and a variable mechanic pressure with

additional nitrogen pressure is applied to make a better contact. The optical system is equipped with 365 nm wavelength exposure optics with an Hg lamp as a light source.

When the sample is illuminated some parts of the resist are exposed and some are not according to the mask design. As a result the mask pattern is created in the resist film. A mask is a sheet of glass, usually partially covered with chromium according to the requirements of design. Exposed parts of the resist were removed by developer MF319 solution as shown in fig. 3.1 (d).Development was done in steps; during these steps resist features were observed by optical microscope to check if fully developed or need of some more development time to obtain wanted feature size.

3.3 Hard bake

Hard bake is the last step of the photolithography process. It is used to drive out water molecules and volatile organic materials from the resist. For hard bake normally a temperature about 120^{o} C for 15 minutes is required. High temperature reduces the photochemical properties of the resist.

3.4 Reactive ion etching

Photolithography is followed by the etching process to create features on a surface as shown in fig. 3.1 (e). To get anisotropic etching of Si pillars, the reactive ion etching (RIE) system T2 from Trion technology was used. The RIE system is extensively used in the microelectronic industry. Both physical (ions) and chemical (radicals) etching behavior are used to etch the surface in the RIE process. Trion (RIE) has a parallel plate diode system and the bottom electrode holds the wafer and is also grounded. A RF (radio frequency) voltage is applied to the upper electrode. The Si etch rate increases by increasing the process pressure and the RF power [17]. The grounded electrode with large negatively self-biased wafer and low operating pressure provides a condition of heavy bombardment of energetic ions from the plasma at the surface of wafer [14].

In contrast to molecular gasses, radicals in plasma are reactive enough to start a chemical reaction. To get anisotropic etching and having good selectivity to resist, $SF_6/O_2/CHF_3$ plasma was used. In that recipe each gas has its own specific function and influence on etching. By changing the flow rate of one of these gasses the etching profile can be controlled. The etching mechanism of RIE could be understood with the help of fig. 3.2.

In the plasma, SF_6 produces the F^- radicals which will take part in chemical etching. First fluorine diffuses into the surface of silicon. These fluorine radicals chemisorbed on the surface of silicon and form SiF. After some chemical reactions, the volatile SiF_4 compound is formed. This compound can easily desorb from the surface in the form of a gas molecule. O_2 creates O^- radicals to form SiO_xF_y molecules which protect the side walls of silicon from being etched.

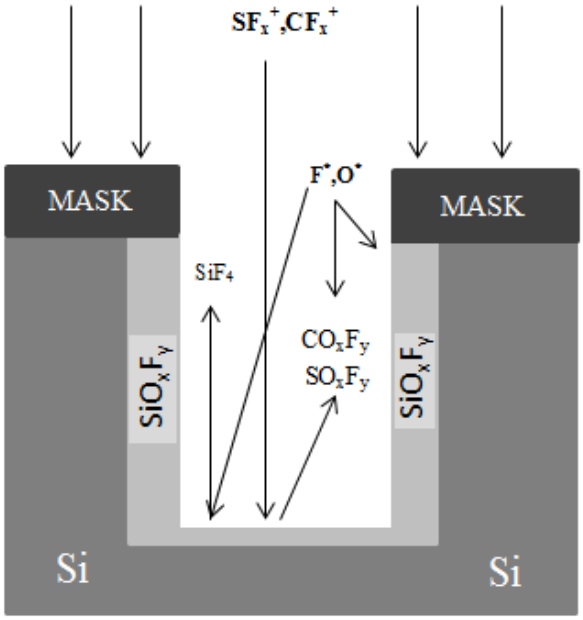

Figure 3.2 *Schematic view of the $SF_6/O_2/CHF_3$ etch process*

To get anisotropic etching and smooth sidewalls CHF_3 gas molecules need to be added because SF_6/O_2 plasmas usually produce rough etched surfaces. CHF_3 ions have the ability to etch SiO_xF_y in one direction and forms volatile CO_xF_y. Similarly, SF_x^+ ions can remove oxy-fluoride by producing volatile SO_xF_y gas [16, 17].

4. CHARACTERIZATIONMETHOD

4.1 Scanning electron microscope (SEM)

The surface of Si pillars was studied by using a scanning electron microscopy (SEM).

A scanning electron microscope (SEM) can produce high resolution images of a sample surface.

The electron column consists of an electron gun and a number of electromagnetic lenses operating in vacuum. The electron gun is used to generate free electrons and electron lenses are used to focus the electron beam on the sample. This fine electron probe is scanned across the surface of the sample. Incident electrons strike and are scattered against the atoms in the specimen. This results in some electron emission from the surface. Usually secondary electrons (SE) and backscattered electrons (BSE) are collected. Secondary electrons emitted with low energy (<50eV) are mostly emitted from regions close to the surface. The brightness of the final image depends on the rate of emitted electrons, which in turn also depends on the slope of surface. For example, normal incidence of the electron beam onto the sample surface results in a low rate of emitted electrons and a darker image. Thus, the angle of incidence was chosen to give more secondary electrons, which results in a brighter image.

The incident electron beam is scanned over the specimen surface and the signal of detected secondary electrons is amplified to give topographic image displays on a TV screen.

4.2 FTIR spectroscopy

The transmittance and reflectance characteristics of Si pillars were investigated by using Fourier Transform infrared spectroscopy (FTIR). The FTIR system is based on the Michelson interferometer principle as shown in fig. 4.1. The beam of broad band infrared radiation from a heated filament is divided into two equal parts by the beam splitter. One of the beams is directed towards a fixed mirror and the other beam towards a moving mirror at the other side of the beam splitter. After hitting the mirrors the beams return back and recombine at the beam splitter and interfere. Part of the resulting beam moves towards detector. For an easy explanation: With the two mirrors (fixed and moving) at the same path length from the beam splitter the two interfering beams are totally in phase and interfere constructively independent of wavelength. This position of the moving mirror is called the point of zero path difference (ZPD). Moving the mirror in any direction by the distance of $\lambda/4$, the path changes by $\lambda/2$ meaning 180^o phase difference so destructive interference for that particular wavelength will be observed. The moving mirror travelling another $\lambda/4$ distance at which the optical path difference is λ gives constructive interference again for that wavelength [18].

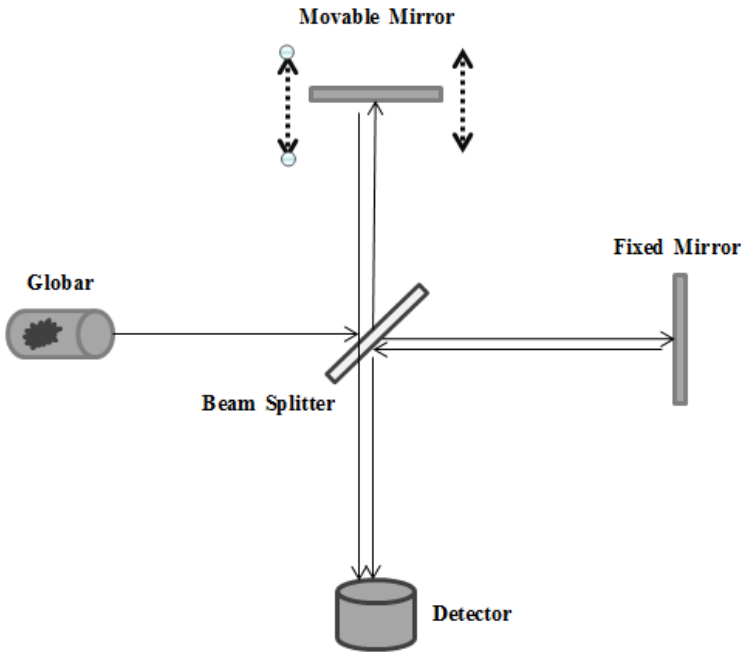

Figure 4.1*: Schematics of conventional Michelson interferometer with a moveable mirror and a stationary mirror having a Globar light source.*

On the way to the detector the beam passes through the sample and the intensity of the beam depends on the difference in path. The intensity *I* of the combined beam is the source of spectral information as a function of path difference. The path difference is dependent on the frequency of incident light. The path difference δ is also known as optical retardation,

$$\delta = n \cdot \lambda_o \qquad (4.1)$$

Where $n \in N = \{0, 1, 2, 3 \ldots .\}$

Eq. 4.1 holds for constructive interference and all light reaches the detector.

For destructive interference, keeping the *n* definition

$$\delta = \frac{2n+1}{2}\lambda_o \qquad (4.2)$$

By changing the position of interferometer mirror an interferogram is measured. The interferogram intensity $I(\delta)$ at the detector is calculated as

$$I(\delta) = 0.5I(\nu_o)cos2\pi\nu_o\delta \qquad (4.3)$$

Each data point of the interferogram gives information about all frequencies originating from the light source where ν_o is the wavenumber ($\nu_o = 1/\lambda$ cm^{-1}) and $I(\nu_0)$ is the interferogram intensity at a particular wavenumber.

All the measurements regarding reflectance and transmittance of Si pillars were obtained by using FTIR. The light source used was a W coil emitting near black body

radiation (Globar). All measurements were performed at room temperature, at atmospheric pressure, and at normal incidence. As a reference a background spectrum was measured to get 100% transmission. The transmission spectrum for bare silicon was measured. The transmission data obtained from bare Silicon was normalized by using background transmission data yielding the transmittance spectrum through only bare Silicon. As a last step the transmission spectrum of silicon pillars was obtained and normalized by using the bare silicon spectrum to get the transmission spectrum of silicon pillars. We assume that the light which was not transmitted to the detector was reflected back [19, 20], since the low doped Si should not absorb IR light.

5. RESULTS AND DISCUSSION

5.1 Results and discussion

In this work wavelength specific resonance enhanced transmission of long wavelength infrared (LWIR) from the silicon (Si) microstructures is measured by using the Fourier transform infrared spectroscopy (FTIR) technique. All measurements are taken at room temperature and atmospheric pressure. Si microstructures are fabricated by using photolithography and dry etching (Reactive ion etching) techniques. The transmission measurements were repeated by varying different parameters (diameter *D*, Length *L*, Pitch *P*) of silicon pillars to check their effects on measurements.

5.2 Transmission through untreated Silicon

Silicon is a low cost optical material with high refractive index [31]. The refractive index of silicon is simply taken as 3.5 [32].

First of all transmission of infrared radiation through untreated silicon (111) was measured. The expected Fresnel reflectance is

$$R = \left(\frac{1-n_{\mathrm{Si}}}{1+n_{\mathrm{Si}}}\right)^2 \qquad (5.1)$$

$$R = \left(\frac{1-3.5}{1+3.5}\right)^2 = 0.30 \qquad (5.2)$$

The reflectance through one interface air/silicon is around 30%. There are two interfaces involved here air/silicon/air. Expected transmission (Eq. 2.14) through the untreated silicon would be

$$(1 - R_1) \times (1 - R_2) \qquad (5.3)$$

$$(1 - 0.3) \times (1 - 0.3) = 0.49 \qquad (5.4)$$

Here R_1 and R_2 are the reflection through the first and second interface respectively.
Fig. 5.1 shows the resultant transmission spectra after normalization of untreated silicon with background.

Fig. 5.1 shows that the untreated silicon transmits about 53% of infrared light almost independent of wavelength. Measured values showed good agreement with the calculated value. IR light simply does not reflect only twice between two interfaces but there are multiple reflections involved. Then the transmission would be

$$(1 - R_1) \times (1 - R_2) + (1 - R_1) \times R_3 \times R_4 \times (1 - R_2) = 0.53 \qquad (5.5)$$

The total transmission through untreated silicon is about 53% which has good agreement with experimental results. There may also be some more effects which can affect the final results like multiple scattering events or detector disability to collect all of the transmitted IR light.

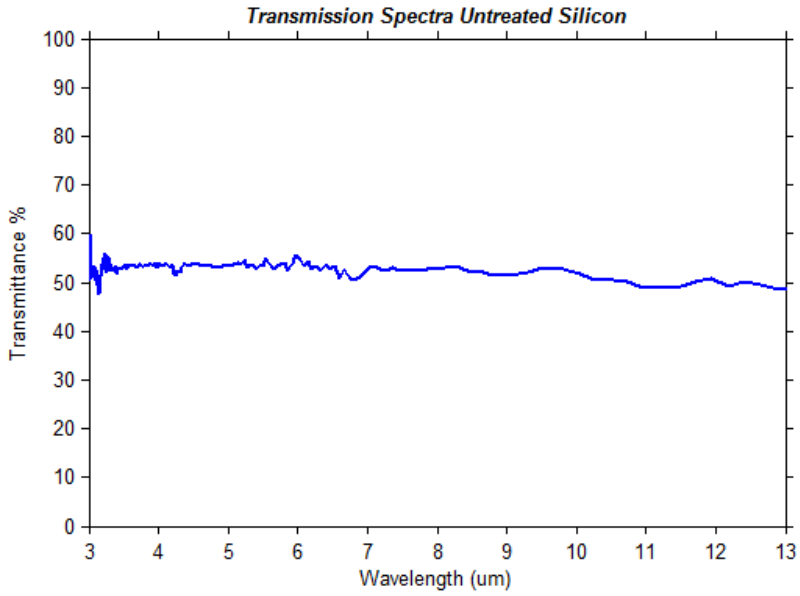

Figure 5.1 *Transmission through plain Silicon (Si) normalized with background shows 53% transmission of IR independent of wavelength.*

During etching the pillars in Si there was an unwanted fluffiness on the surface of pillars examined. This effect occurs due to the sample heating during etching in RIE which makes the surface passivation polymers unstable. To make transmission calculation more correct I have placed plain silicon without any pattern along the sample with patterns for etching in RIE to make its surface rough; this is used for normalization to minimize the error in the results. Fig. 5.2 shows the comparison between the transmission of plain Si and rough Si surfaces; experimental results show that both have a comparatively equal transmission independent of wavelength. This indicates that the surface roughness is too small to make any noticeable difference in transmission.

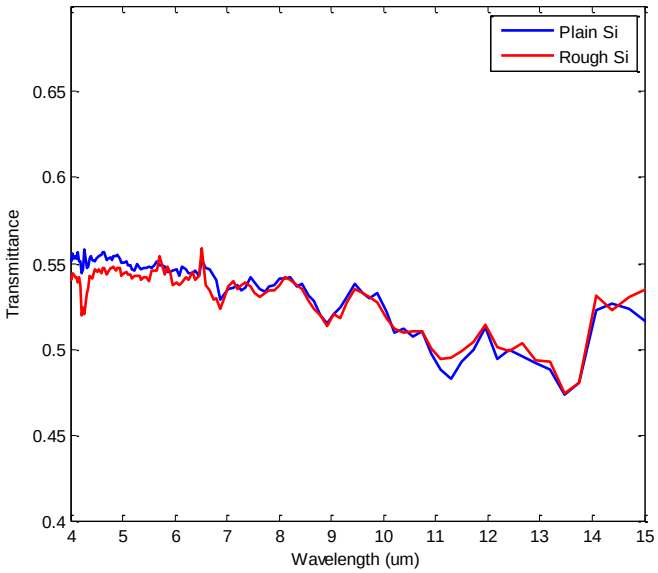

Figure 5.2 *Transmission spectra of plain Si and rough Si. Transmission spectrum shows that both have nearly equal transmission.*

5.3 Transmission through the Si pillars

We have studied the resonance enhanced wavelength specific transmission of IR light from Si pillar array by a controlled variation in pillar diameter. The length and pitch is also changed systematically in a controlled manner. In that way a tunable wavelength specific resonance enhanced transmission of LWIR can be achieved. The Si pillars of diameter *D* and length *L* are placed in a triangular array with a pitch *P*.

The transmitted wavelength related to a specific diameter can be associated with the condition for constructive interference [33],

$$\lambda = \frac{\pi(D/2)n_P}{m} \qquad (5.6)$$

Where λ is the wavelength associated with the diameter of the pillar, *D* is the diameter of the pillar, n_P is the refractive index of the pillar and *m* is an integer. Constructive interference in the cross section where *m*=1 corresponds to the fundamental waveguide mode (HE11).

Here, we show experimentally and theoretically the specific wavelength enhanced transmission by changing the diameter of the Si pillars. Simulations are run by Nicklas Anttu (Division of Solid State Physics, Department of Physics, Lund University) for Si (*n*=3.5) region to show transmission in actual structure in non-absorbing region. Simulations are performed for single interface, ignoring backside reflection. Fig. 5.3 below shows the simulation schematics for *D*=1 μm, *P*=7 μm and *L*=5 μm.

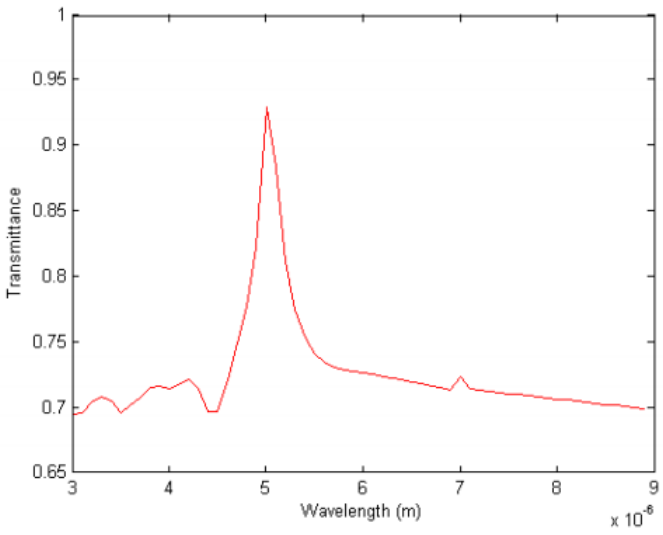

Figure 5.3 *Simulation result for a silicon pillar array having D=1 μm, P=7 μm, L=5 μm. Here the pitch is larger than the resonance wavelength and a sharp peak is observed due to an overlap of incident light with the resonance mode.*

This shows a resonance peak at the wavelength 5 μm. Here, the pitch *P* is larger than the resonance wavelength. The sharp resonance peak in transmittance is probably due to the good overlap of incident light with the HE11 resonance mode. If the pitch *P* is larger than the resonance wavelength, the peak in transmittance becomes narrow.

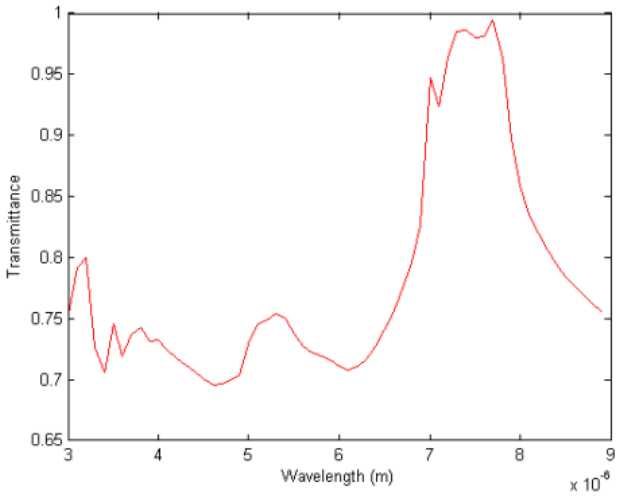

Figure 5.4 *Simulation result for a silicon pillar array with D=1.5 μm, P=7 μm and L=5 μm. Here the pitch is comparable with the resonance wavelength and a clear peak is observed in transmittance due to waveguide resonance.*

Fig. 5.4 shows the simulation spectrum for the parameters *D*=1.5 μm, *P*=7 μm and *L*=5 μm. We can observe a clear peak in transmittance at 7.5 μm and the transmittance value reaches very close to one. As the pillar diameter is increased, the resonance peak shifts to higher wavelength in transmittance. This resonance peak is due to the waveguide resonance. As the pitch *P* is similar to the resonance wavelength, a clear transmittance peak shows up at waveguide resonance.

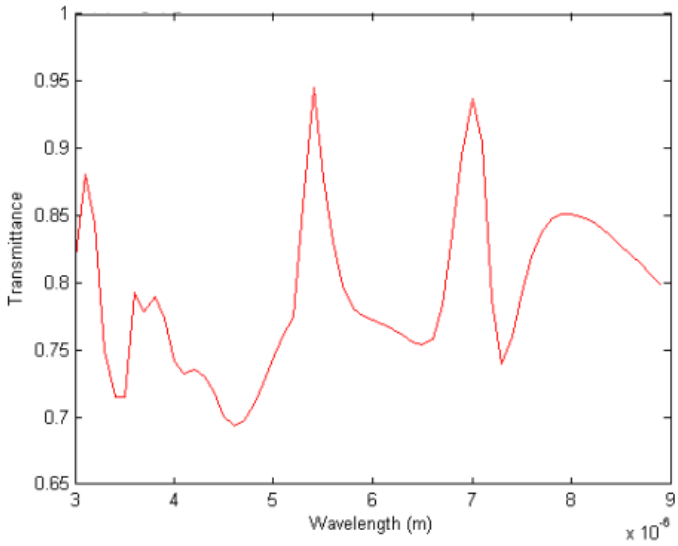

Figure 5.5 *Simulation result for a silicon pillar array having D=1.5 μm, P=5 μm and L=5 μm. Here the pitch is smaller than the resonance wavelength and additional peaks are observed due to coupling effect.*

Fig. 5.5 shows the transmission simulation spectrum for *D*=1.5 μm, *P*=5 μm and *L*=5 μm. Here, we can observe a narrow peak in transmittance close to 7 μm with some additional structure also present in the plot. We do not see a clear peak due to

waveguide resonance. It should be due to the short distance between pillars with a pitch P=5 μm. With D=1.5 μm, the resonance transmission is expected close to the wavelength 7 μm but a small pitch coupling effect has introduced some additional structures. That is the third case when the pitch P is smaller than the resonance wavelength and some additional structures show up in the spectrum.

Here we need to correct the pillar diameter so that light can couple to HE11 mode, which is most important for the peak. The pitch of the pillars causes coupling between the modes of neighboring pillars impact peaks, which is enough to see a resonance peak. If the pitch of pillars remains the same throughout the sample then it enhances the effect of resonance peak. But the specific pitch throughout the sample is not necessary to see the resonance peak. For the absorption of light in nanowire array for a fixed diameter, the length $L$and pitch P has strong direct relation with each other [38]. So with the increase in length L of Si pillar the pitch P should also increase in order to see a good coupling between the modes of neighboring pillars.

We design and fabricate large scale vertical silicon pillar arrays as shown in fig. 5.6 (b), a SEM image tilted at 30^o. We have fabricated arrays of pillars with diameters varying from 1.33 μm ± 36 nm to 2.48 um ± 62 nm and a constant pitch and length of 7 μm and 5 μm respectively.

Fig. 5.7 shows the experimental results of the resonance enhanced transmission for P=7 μm, L=4.2 μm and a pillar diameter of 1.33 μm ± 36 nm, the uncertainty taken as the standard deviation (Fig. 5.6 (a)).Transmission measurements of Si pillars are performed by illuminating with the Globar LWIR source at normal incidence. The pitch is comparable to the resonance wavelength. Si pillar array shows the coupling effect at wavelength 6.2 μm, which is reasonably close to the calculated value. The transmission reaches 76% at a particular wavelength.

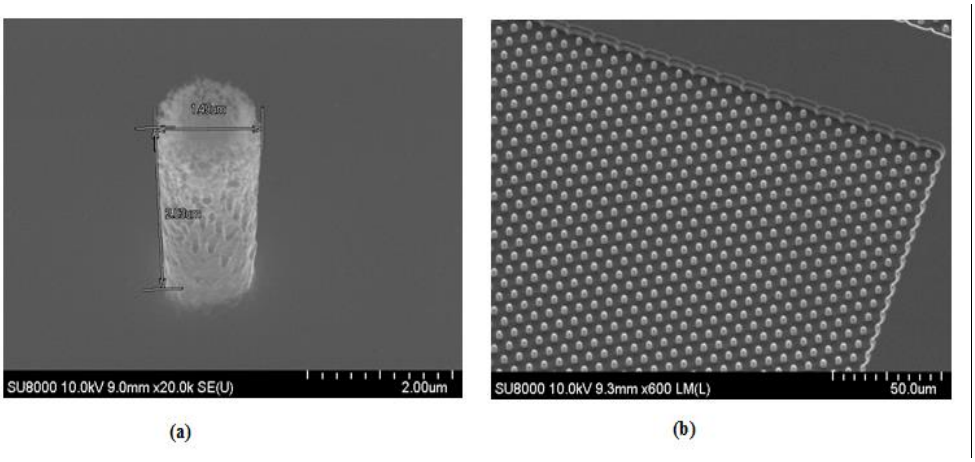

Figure 5.6 *(a) Patterned vertical silicon pillar; SEM image taken at 30^o tilt position. Mean pillar diameter is 1.33 μm ± 36 nm, length is ~4.2 μm and pitch 7 μm. (b) Arrays of Si Pillars.*

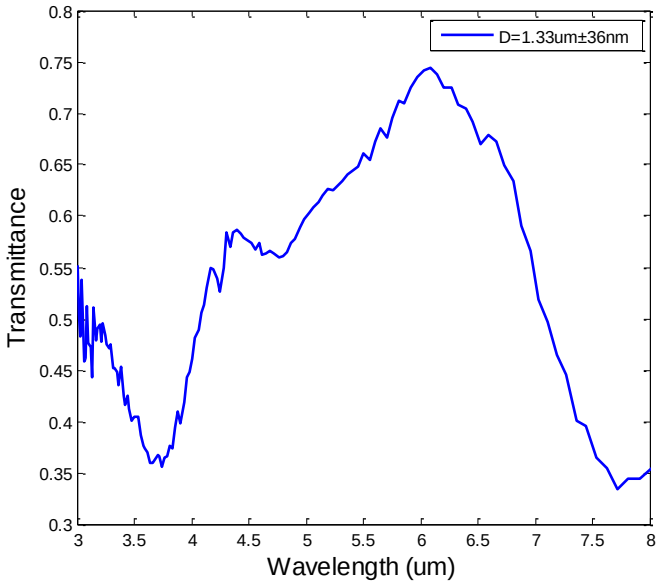

Figure 5.7 *Experimental data for a silicon pillar array having D=1.33 μm ± 36 nm, P=7 μm, L=4.2 μm. Here the pitch is comparable with the resonance wavelength and a clear peak is observed in transmittance due to waveguide resonance at wavelength 6.2 μm and transmission of 76%.*

The position of the transmission peak can be tuned over the wide range of IR band by adjusting the diameter of pillars. To remove the substrate contribution from the final result, we have normalized the transmission through pillar and substrate with the silicon sample having a rough surface. Because the walls of pillars and also the surface between the pillars is not smooth, to normalize with untreated plain Si is not a good option. The roughness of the surface is achieved by etching it with RIE for couple of minutes. The final spectra show the intensity of transmitted light through the Si pillars only.

In fig. 5.9 we present the transmittance of arrays with larger pillar diameter as compared to the case in fig. 5.7 discussed above. Here L=4 μm, P=7 μm and D= 1.42 μm ± 35 nm (Fig. 5.8).The silicon pillar array shows the coupling effect at wavelength 7.5 μm, which is reasonably close to the calculated value. The transmission reaches 77% at a particular wavelength. With the increase in pillar diameter, the peak shifts towards higher wavelength in the IR band. The simulated spectrum (fig. 5.4) is quantitatively in good agreement with the experimental results with respect to the spectral peak position as a function of pillar diameter. The peak is low in the experimental result compared to the simulated spectrum, which could be due to multiple scattering of light through the substrate so that detector cannot collect all scattered light. Here we can observe a linear dependence of peak position with the pillar diameter.

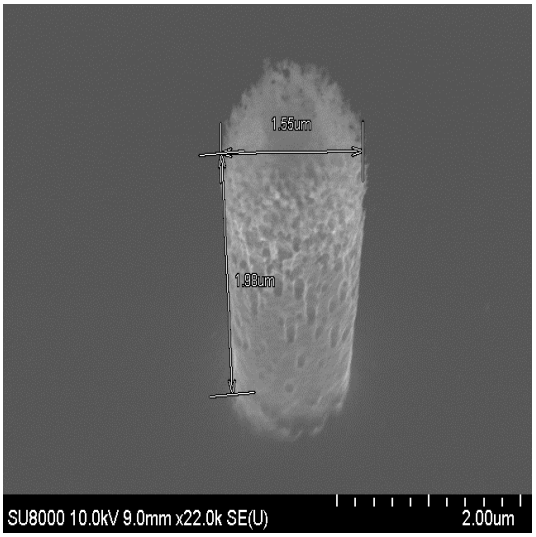

Figure 5.8 *Patterned vertical Si pillar SEM image taken at 30^o tilt position. The mean diameter of pillars is 1.42 um ± 35 nm, length is ~4 μm and pitch 7 μm.*

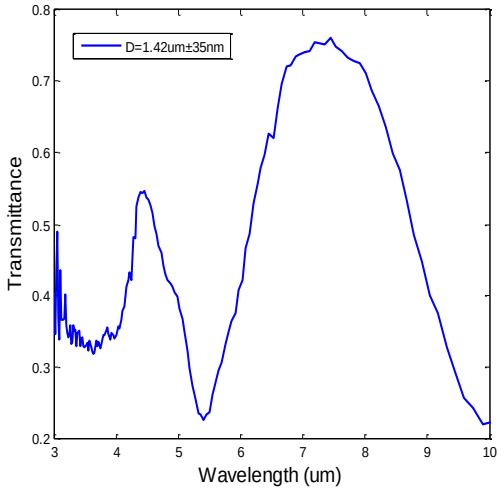

Figure 5.9 *Experimental data result for a Si pillar array having D=1.42 um ± 35 nm, P=7 μm and L=4 μm. Here the pitch is comparable with the resonance wavelength. A clear peak is observed in transmittance due to waveguide resonance at wavelength 7.5 μm.The transmission is about 77%.*

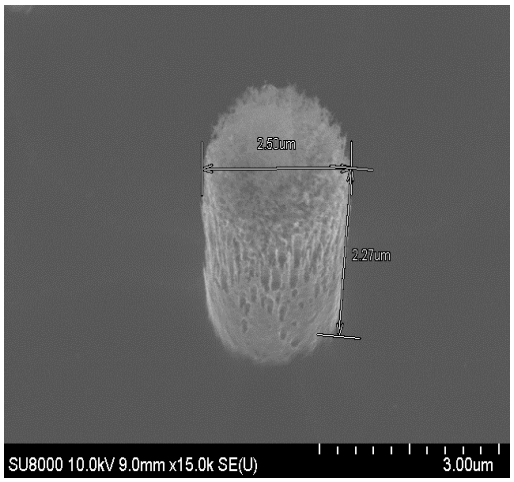

Figure 5.10 *Patterned vertical Si pillar; the SEM image is taken at 30^o tilt position. Mean pillar diameter is 2.48 μm ± 62 nm, the length is ~4.5 μm and pitch 7 μm.*

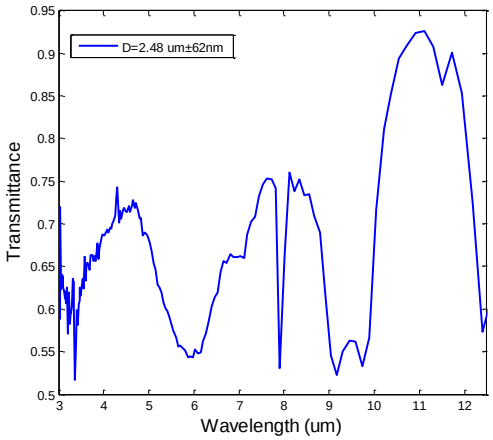

Figure 5.11 *The experimental data result for a Si pillar array having D=2.48 μm ± 62 nm, P=7 μm and L=4.5 μm. Here the pitch is smaller than the resonance wavelength and additional peaks are observed due to coupling effect. A strong transmission peak at wavelength 11 μm is observed with 94% transmittance.*

Fig. 5.11 shows the transmission spectrum with pillar dimensions as L=4.5 μm, P=7 μm and diameter D=2.48 μm ± 62 nm (Fig. 10). Here we can observe that with the increase in diameter, the transmission peak shifts towards higher wavelength in the IR band. Transmission reaches to 94% at a wavelength λ=11 μm. Here some additional structures are also present due to the coupling effect as a result of the small pitch.

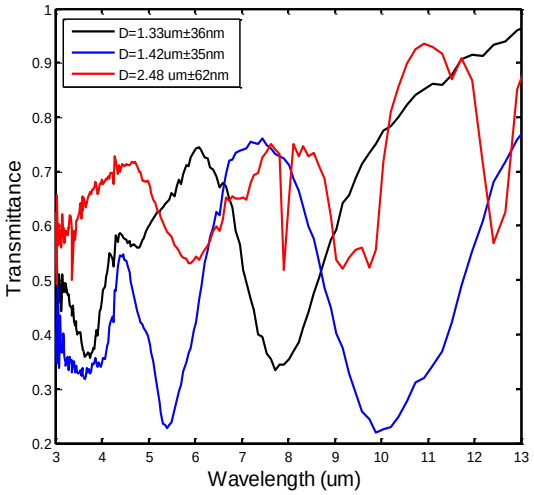

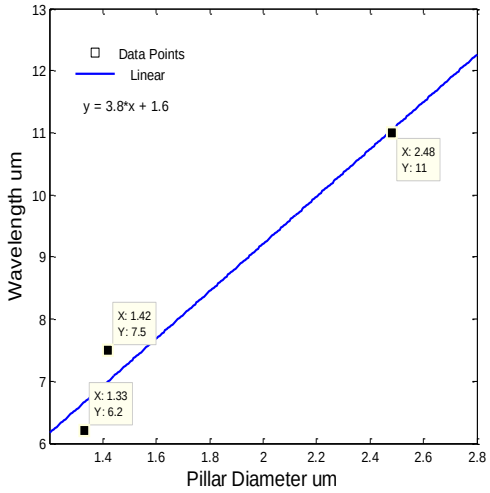

Figure 5.12 (a) *Comparison between three different diameter sizes of Si pillars. By increasing the diameter, the enhanced transmission peaks shift linearly towards the higher wavelengths.*

Figure 5.12 (b) *Enhanced transmission of IR at a specific diameter of Si Pillars fit to a linear model.*

Fig. 5.12 (a) shows the comparison of transmission spectra of pillars having different diameters but the same pitch. Here we can observe that with increasing the diameter the transmission peaks shift towards higher wavelengths.

Fig. 5.12 (b) shows the data points of resonance enhanced transmitted wavelength at a specific diameter of Si pillar fit to a linear model. The line has a linear relation $Y = (3.8 \times X) + 1.6$. The general form of linear equation is $Y = mX + b$. In this equation m and b are constants where m determines the slope of that line and constant b is known as Y intercept. According to this model we can tune the transmitted light at a specific wavelength by tuning the pillar diameter.

In figure 5.13a simulated demonstration shows the electric field intensity distribution of the HE11 mode as a function of nanowire diameter inside the wire. Figure 5.13 is for InAsSb nanowires embedded in resist. Si pillars should show the similar results for the transmission of IR light. It explains the optical response of three different pillar diameters.

Fig. 5.13 (b) shows the case in which the wire diameter D = 700 nm is comparable with associated transmitted wavelength λ = 4.5 μm. At the absorption peak, due to resonance excitation of the HE11 waveguide mode, a strong field strength inside the wire is observed [36]. Results should be similar for the transmission spectra of Si pillars. The fundamental HE11 resonance mode can be tuned across the broad spectral

range, and selection of different pillar diameters can exhibit high wavelength selectivity [37]

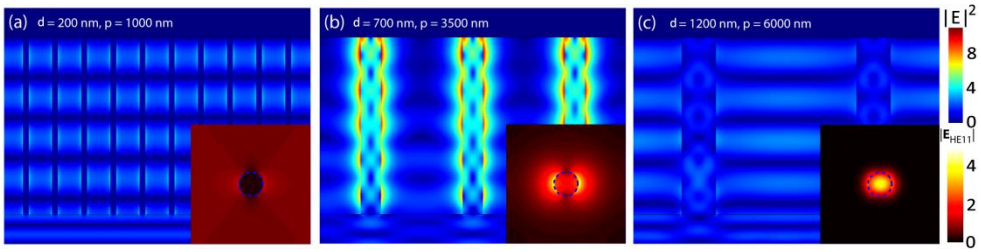

Figure 5.13 *Electric field intensity inside the InAsSb nanowires embedded in resist having three different diameters; (a) Due to small diameter pillar shows the field strength outside the wire and the wavelength enhanced coupling is weak. (b) Increased diameter of wire leads to the resonant excitation of HE11 mode; as a result high field intensity inside wire is achieved. (c) Further increase in the wire diameter leads to the localization of HE11 mode in the middle of the pillar. Due to small overlap, small coupling occurs, which means weak resonance enhanced absorption of light [36]. In this work we are using Si pillars and the transmission results should be similar as discussed for absorption.*

Fig. 5.13 (a) shows the case with small diameter; it exhibits weak overlap and coupling between HE11 mode and incident plane wave. Due to the small diameter the maximum field strength is outside the wire and enhanced transmission of coupled wavelength is weak. As a result absorption would be lower. In our case transmission would be lower.

Fig. 5.13 (c) shows the case when the wire diameter is comparatively larger than the previous two cases. Due to large diameter the field strength due to HE11 mode is localized in the middle of wire. The overlap between field generated by HE11 mode and incidence plane wave is weak. Small amount of coupling can be achieved and in the result weak absorption is observed. If the pillars are close enough the HE11 mode couples together and transmission peaks begin to broaden.

5.4 Some lithography results

During photolithography, the mask should be in contact with the flat surface of resist film to get maximum resolution of exposure. Figures 5.14 (a) and (b) show the SEM images of pattern features of resist on Si surface resulting in good contact between mask and resist film. In another case, when edge bead causes unwanted gap between mask and the flat surface of the resist during exposure, doughnut shaped features are observed on the surface of Silicon. These doughnut shaped features are produced due to the Fresnel diffraction limit. After etching these doughnut shaped features result in hollow Si pillars.

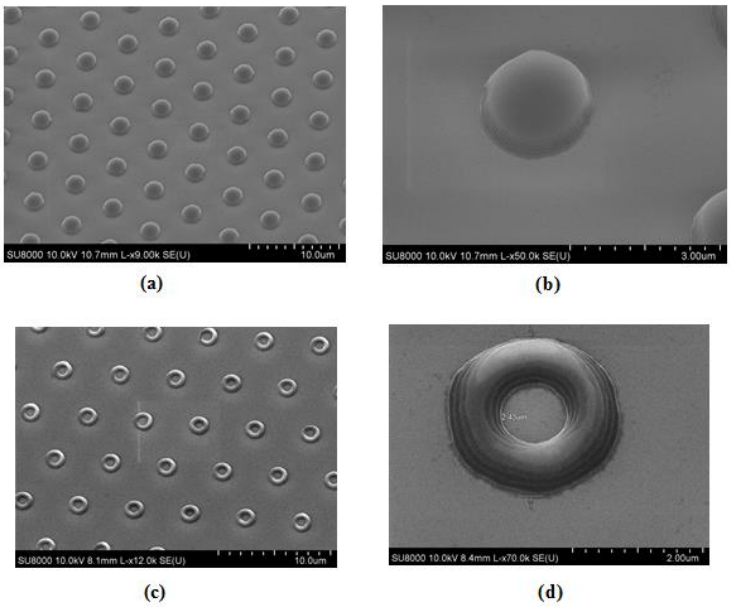

Figure 5.14 *SEM image taken at 30^o tilt position; (a) and (b) show the solid features on Si surface as a result of photolithography, while (c) and (d) show the doughnut shaped features on Si surface as a result of photolithography.*

Hollow Si pillars also have interesting optical properties. Fig. 5.15 shows the simulation results of hollow Si pillars having height L=5 μm, pillar diameter D_1= 2.47 μm, inner core diameter D_2=1.48 μm and having two different pitches P=7 μm and P=5 μm. Simulation results show that light should be able to transmit through hollow Si pillars.

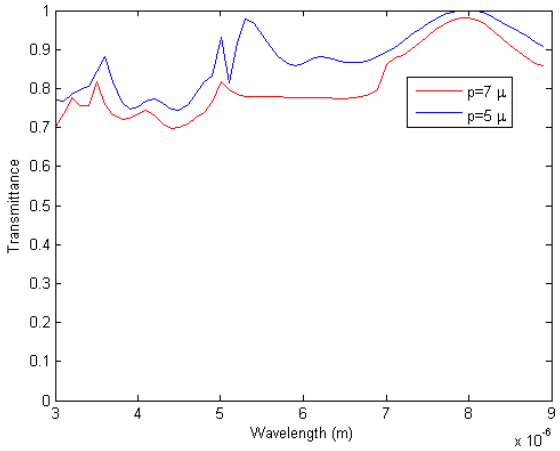

Figure 5.15 *Simulation result for a Silicon pillar array having pillar diameter D_1=2.42 μm, inner core diameter D_2=1.48 μm, length L=5 μm and pitches P=7μm and 5μm, respectively.*

Fig. 5.16 (b) shows the transmission spectrum of hollow Si pillars having pillar diameter D_1=2.47 μm, inner core diameter D_2=1.48 μm, pitch P=5 μm and height L=4 μm. In this case the pitch is small compared to the pillar diameter. The HE11 mode

couples together and the transmission peak would be broad. Transmission spectrum shows the maximum transmission at wavelength λ=8 μm.

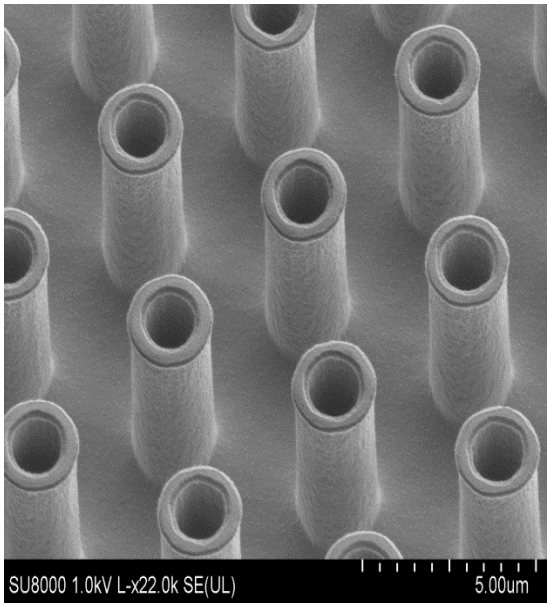

Figure 5.16 (a) *Si hollow pillar array having pillar diameter D_1=2.42 μm, inner core diameter D_2=1.48 μm, pitch P=5 μm and L=4 μm. SEM image is taken at 30^o tilt position.*

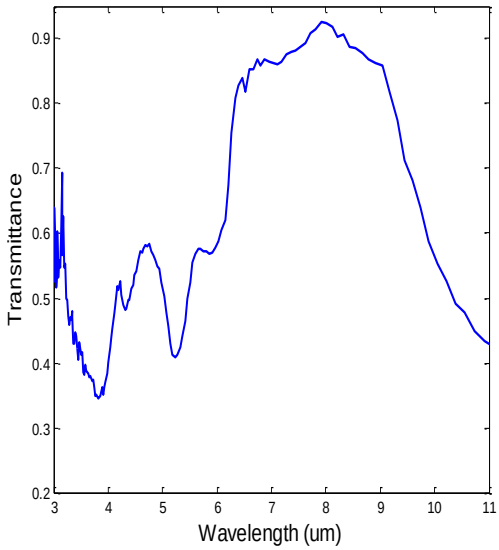

Figure 5.16 (b) *Experimental data result for a Si hollow pillar array having pillar diameter D_1=2.42 μm, inner core diameter D_2=1.48 μm, pitch P=5 μm and length L=4 μm. The transmission spectrum shows maximum transmission at wavelength of λ=8 μm. A broad peak can also be observed.*

Fig. 5.18 shows the transmission spectrum of hollow Si pillars having pillar diameter D_1=1.75 μm, inner core diameter D_2=1.2 μm, pitch P=7 μm and height L=2 μm. We cannot see any clear resonance peak due to the small length of hollow pillar as compared to the pitch of pillars. There is week coupling between the neighboring pillars impact peak.

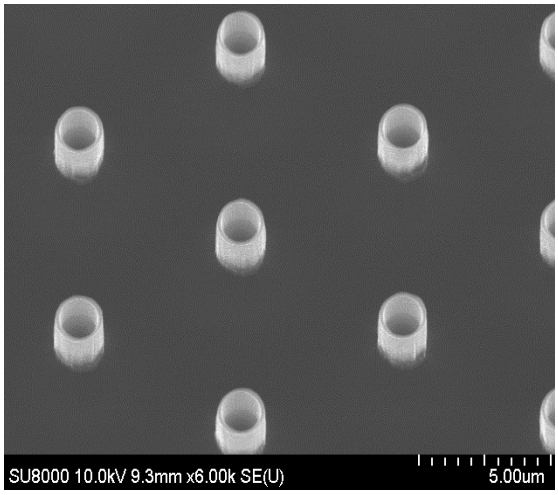

Figure 5.17 *Si hollow pillar array having pillar diameter D_1=1.75 μm, inner core diameter D_2=1.2 μm, pitch P=7 μm and L=2 μm. SEM image is taken at 30^o tilt position.*

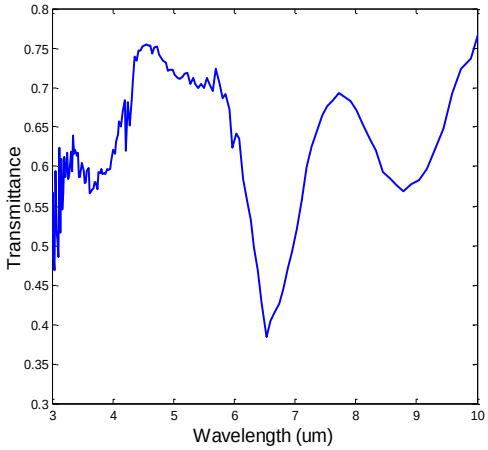

Figure 5.18 *Experimental data result for a Si hollow pillar array having pillar diameter D_1=1.75 μm, inner core diameter D_2=1.2 μm, pitch P=7 μm and length L=2μm. The transmission spectrum did not show clear peak due to the small height of pillars.*

Conclusion

By using photolithography and RIE Si pillars were created on Si substrates. We have demonstrated the resonance enhanced wavelength specific transmission of LWIR by using transmission measurements through Si pillars with FTIR spectroscopy. Transmission peaks are due to the fundamental waveguide HE11 mode. Results show that the position of the transmission peak is highly dependent on geometrical parameters of Si pillars. By doing control variation in diameter, pitch and length of Si pillars, the resonance enhanced transmission peak can be shifted to higher or lower wavelength. We can conclude that the tunable transmission of IR light through Si pillars is highly diameter dependent. Due to high resonance enhanced wavelength specific transmission through Si pillars, these structures can be used in back side illuminated InAsSb nanowire infrared photodetectors.

Bibliography

[1] JinsuYoo, Junsik CHO, Kyumin Han, Junsin Yi, "*RIE surface texturing for optimum light trapping in multicrystalline silicon solar cells*'' Journal of Korean Physical society, Vol.60, No. 12, 2071-2074 (2012)

[2] Yung-Jr Hung, San-Liang Lee, Kai-Chung Wu, Yian Tai and Yen-Ting Pan "*Antireflective silicon surface with vertical-aligned silicon nanowires realized by simple wet chemical etching process*''. Vol. 19, No. 17, optics express 15802 (2011)

[3] Daniel H. Raguin and G. Michael Morris, "*Antireflection structured surfaces for the infrared spectral region*''. J. Applied optics, Vol. 32, No. 7, 1154-1167, (1993)

[4] Yung-Jr Hung, San-Liang Lee, and Larry A. Coldren, "*deep and tapered silicon photonic crystals for achieving anti-reflection and enhanced absorption*,'' Vol. 18, No. 7, J. optics express, 6841-6852 (2010)

[5] Dr. Michael Fink, "*types of antireflective treatments and when to use them*,'' the photonic solutions update, 28-31.

[6] Ali Seerpenguzel, Adnan Kurt, Ibrahim Inance, James E. Cary, and Eric Mazur, "*Luminescence of black silicon,'' Journal of Nano photonics''*, Vol. 2, 021770 (2008).

[7] Jean-Baptiste Bruckner, J. L. Rouzo, L. Escoubas, G. Bergins, C. Gourgon, O. Desplats, and J. J. Simon, "*Flat top and patterned topped cone gratings for visible and mid infrared antireflective properties*,'' Vol. 21, No, 13, Optics Express 16043-16055 (2013)

[8] R. Bouffaron, L.Escoubas, J.J. Simon, Ph. Torchio, F. Flory, G. Berginc, Ph. Masclet, C. Perret, P. Schiavone, " *Design and fabrication of infrared antireflecting bi-pitchic micro-structured surfaces'' Micro-optics'',* Vol. 6992, 69920H, (2008).

[9] R. Bouffaron, Escoubas, J.J. Simon, Ph.Torchio, F. Flory, G. Berginc, and Ph. Masclet, "*Enhanced antireflecting properties of micro-structured top-flat pyramids*,'' Optics Express, Vol. 16, No. 23, 19304-19309, (2008).

[10] NicklasAnttu, "*Nanophotonics in absorbing III-V nanowire arrays*''ISBN 978-91-7473-549-9, doctoral thesis, (2013)

[11] David J. Griffiths, "*Introduction to electrodynamics*'' 3rd ed. ISBN 0-13-805326-X

[12] Harry J. Levinson, "*Principles of lithography*'', 2nd ed. ISBN 0-8194-5660-8

[13] http://nanofab.ece.cmu.edu/resources/s1800seriesDataSheet.pdf

[14] May, Gray, S., Simon M. Sze, "*Fundamentals of semiconductor fabrication*'', ISBN 0-471-23279-3, Wiley international edition ISBN 0-471-45238-6.

[15] http://www.microchemicals.com/downloads/application_notes.html

[16] H. Jansen, M. de Boer, R. Legtenberg and M. Elwenspoek, *"the black silicon method: a universal method for determining the perameter setting of a fluorine-based reactive ion etcher in deep silicon trench etching with profile control*'', J. Micromech. Microeng.5, 115-120, (1995).

[17] R. Legtenberg, H. Jansen, M. de Boer, and M. Elwenspoek, *"anisotropic reactive ion etching of Silicon using $SF_6/O_2/CHF_3$ gas mixtures*'', J. Electrochem.Soc., Vol. 142, No. 6, (1995).

[18] F. A. Settle, "*hand book of instrumental techniques for analytical chemistry*'' ISBN 0-13-177338-1.

[19] Adrian Gagnon, "*development of a Si based resonant cavity enhanced infrared photodetector*'', Thesis master of applied science, McMaster University Hamilton, (2012).

[20] Martina Reithmeier, *"antireflecting interlayers for enhancing transparency of metal layers for internal reflection infrared spectroscopy*'', Department of interface chemistry and surface Engineering, Max plank Institute for Eisenforschung, Dusseldrof, Germany. (2011)

[21] A. Rogalski, "*History of infra red detectors*'' J. opto-Electronics Review 20(3), 279-308, (2012).

[22] E.S. Barr, "*Historical survey of the early development of the infrared spectral region*,'' Amer. J. Phys. 28, 42-54 (1960)

[23] T. W. Case, "*Notes on the change of resistance of certain substrates in light*,'' Phys. Rev. 9, 305-310, (1917).

[24] A. Rogalski, "*infrared detectors,'' Electrocomponent science monographs*, Vol. 10, Amsterdam, Gordon and Breach Science Publishers, 2000 ISBN 9056992031.

[25] Donald A. Neamen, "*Semiconductor physics and devices, basic principles*,'' 3rd ed., Published McGraw-Hill, ISBN 0-07-232107-5.

[26] A. Rogalski, "*Infrared detectors: an overview*,'' J. Infrared physics &technology 43, 187-210, (2002).

[27] Lewis Fraas, Larry Partain, "*Solar cells and their applications*,'' 2nd ed. John Wiley & sons, ISBN 978-0-470-44633-1

[28] The Landolt-Börnstein database, Springer Materials.

[29] NicklasAnttu, "*Geometrical optics, electrostatics, and nanophotonic resonances in absorbing nanowire arrays*,''J. Optics letters, Vol. 38, No. 5, (2013).

[30] K. Seo, M. Wober, P. steinvurzel, E. Schonbrun, Y. Dan, T. Ellenbogen and K. B. Crozier, "*Multicolored Vertical Silicon Nanowires*,'' J. Nano letters, 11, 1851-1856, (2011).

[31] D. S. Hobbs and B. D. MacLeod, "*Design, fabrication and measured performance of anti-reflecting surface textures in infrared transmitting materials*,'' SPIE 5786-40, (2005).

[32] www.LatticeMaterials.com, (Lattice materials LLC, 516 E Tamarack St., Bozeman, 2011).

[33] NicklasAnttu, K. L. Namazi, P.M. Wu, P. Yang, H. Xu, H. Q. Xu and U. Hakanson, "*Drastically increased Absorption in vertical semiconductor nanowire arrays: A non abrorbing dielectric shell makes the difference*,'' J. Nano Res., 5(12), 863-874, 2012,

[34] F. J.Garcia-Vidal, J. M. Pitarke, and J. B. Pendry, *"effective medium theory of the optical properties of aligned carbon nanotubes*,'' J. Physical Review letters, 78, 4289 (1997).

[35] P. M. Wu, N. Anttu, H. Q. Xu, L. Samuelson and M-E. Pistol, "*colorful InAs nanowire arrays: from strong to weak absorption with geometrical tuning*,'' J. Nano Letters, 12, 1990-1995, (2012).

[36] J. Svensson, N. Anttu, N. Vainorius, B. Mattias Borg, and L. E. Warnersson, *"Diameter dependent photocurrent in InAsSb Nanowire Infrared photodetectors*,'' Nano Letters, 13, 1380-1385, (2013).

[37] B. Wang and P. W. Leu, "*Tunable and selective resonant absorption in vertical nanowires*,'' J. Optics Letters, Vol. 37, No. 18, 3756-3758, (2012).

[38] N. Anttu and H. Q. Xu, "Efficient light management in vertical nanowire arrays for photovoltaics,'' J. Optics Express, No. S3, Vol. 21, A558-A575, (2013)

[39] http://www.sinosauna.com/infrare.aspx